Time-scale matching in the response of a leaky integrate-and-fire neuron model to periodic stimulus with additive noise

T. Shimokawa, K. Pakdaman, and S. Sato
Department of Human and System Science, Graduate School of Engineering Science, Osaka University, Toyonaka 560-8531, Osaka, Japan
(Received 30 September 1998)

We study the response of a leaky integrate-and-fire neuron model to subthreshold periodic stimulus with additive noise. Previous works have shown that the interspike interval distribution at the modulation period goes through a maximum with increasing either the noise intensity or the period. This maximum appears when the stimulation period is close to the mode of the interspike interval distribution in the absence of the modulation. This phenomenon is called time-scale matching. In this paper, we examine time-scale matching in the response to periodic signals with and without resetting of the input phase at each firing. For the case without resetting, we calculate the phase distribution by iterating a stochastic phase transition operator. This operator extends the phase transition curve commonly used in the analysis of the response of deterministic oscillators to periodic stimulation. We also examine the dependence of the time-scale matching on the input amplitude. Furthermore, we consider the response of the system in the frequency domain. It is known that the signal-to-noise ratio derived from the power spectral density goes through a maximum with increasing noise intensity. We show that the signal-to-noise ratio also has a hump as a function of the period, and discuss its relation to time-scale matching. This work helps in clarifying conditions whereby noise can improve the detection of a weak periodic signal by neurons through time-scale matching. [S1063-651X(99)07703-X]

PACS number(s): 87.10.+e, 07.05.Mh

I. INTRODUCTION

Experimental and theoretical investigations have shown that noise of appropriate amplitude can enhance signal transmission in nervous systems, for instance, by linearizing the response to suprathreshold stimulation (for a review, see [1]), by increasing input-output correlation, coherence, and transinformation in the presence of weak aperiodic stimulation [2], or enabling the detection of subthreshold periodic signals [3,4]. The last phenomenon is one form of stochastic resonance (SR) [5,6], i.e., ''a phenomenon that is manifest in nonlinear systems whereby generally feeble input information (such as a weak signal) can be amplified and optimized by the assistance of noise'' [6].

SR has been thoroughly studied in noisy weakly periodically modulated systems in a double-well potential (for reviews, see [5,6], and references therein). It has been suggested that SR can occur through matching between the rate of the noise-induced hopping between the two stable states and the modulation period (for a discussion of this issue, see [5–7]).

Some neurons in nervous systems operate as bistable devices, so that the aforementioned studies on SR can be directly extended to them. However, under many circumstances, including some of the experiments described in [3], sensory neurons are not bistable, but rather excitable, that is, they have a single resting state, small perturbations of this state are damped, while large stimulations evoke an action potential followed by a return to the stable state. Therefore, in order to get a better understanding of the mechanisms underlying SR-like phenomena in nervous systems, the results obtained in the case of bistable systems need to be reformulated and extended to excitable systems [8]. The purpose of this work is to examine this issue in a prototype of an excitable system. More precisely, we investigate whether time-scale matching enhances signal detection in the leaky integrate-and-fire model (LIFM). This model captures essential aspects in neuronal behavior, namely, excitability—leading to an all-or-none response—and refractoriness—progressive recovery of excitability following a discharge. Therefore, the study of the dynamics of the LIFM can help in elucidating the mechanisms underlying the beneficial roles played by noise in signal transmission and processing in nervous systems.

The study of SR-like phenomena in the LIFM was initiated in [9,10]. In [9], Bulsara *et al.* studied noise-enhanced detection of a weak periodic signal in the LIFM. More precisely, they showed that the peak heights of the interspike interval (ISI) distribution go through a maximum with increasing the modulation period T or noise intensity D thereby exhibiting ''resonance'' phenomena. Furthermore, they showed that both humps occur when T is close to the mode of the ISI distribution without modulation, thus providing strong evidence for time-scale matching in these resonances.

In this paper, we extend their results by systematically investigating the influence of noise intensity, modulation period, and amplitude on time-scale matching. In this way, we shed light on the role of subthreshold modulation characteristics, and we determine conditions under which time-scale matching occurs. Furthermore, the results in [9] were obtained under the assumption that the input phase is reset after each discharge. Physiologically, this may correspond to endogenous membrane potential modulation [11]. It can also provide an approximation for exogenous forcing, i.e., when the input phase is not reset. We propose a method for the computation of the distribution of discharge phases when the input phase is not reset. Our method relies on the extension

of the phase transition curve commonly used in the study of periodically forced deterministic oscillations to a noisy system. Using the phase distribution, we compute the ISI distribution of the exogenously forced LIFM. This allows us to compute conditions for time-scale matching in this system and compare them with those in the endogenously forced LIFM.

The study in [9] deals mainly with the response of the LIFM in the time domain. In [10], Plesser and Tanaka examined the response of the noisy LIFM to subthreshold periodic forcing in the frequency domain. To this end, they computed the signal-to-noise ratio (SNR) from the power spectral density (PSD) of the spike train, and showed that this quantity was maximized at some intermediate noise level. In this work, we investigate whether this maximum results from time-scale matching. Furthermore, in the same way as in the time domain, we examine the influence of the modulation period and amplitude to determine whether the SNR is also maximal at some appropriate forcing period. Finally, we compare the results in the time and frequency domains.

This paper is organized as follows. In Sec. II, we introduce the LIFM. In Sec. III, we propose methods to analyze the response with and without resetting of the input phase. In Sec. IV, we examine the time-scale matching and investigate the influence of the modulation amplitude. In Sec. V, we investigate the response of the system in frequency domain. Finally, we discuss our results in Sec. VI.

II. LEAKY INTEGRATE-AND-FIRE NEURON MODEL

A. Deterministic model

The LIFM describes the electric activity of a neuron membrane. It is composed of a resistance and a capacitance in parallel, together with a firing threshold. The subthreshold dynamics of the membrane potential $V(t)$ is described as follows:

$$C\frac{dV(t)}{dt}=-\frac{V(t)-V_\infty}{R}+I(t), \quad V(t)<S_0 \tag{2.1}$$

$$V(t^+)=V_0<S_0 \quad \text{if} \quad V(t)=S_0,$$

where R is the total membrane resistance, C the total membrane capacity, V_∞ the resting potential, V_0 the resetting potential, $I(t)$ the stimulus current, and S_0 the constant firing threshold. This model generates a discharge when V exceeds S_0, which is described by an impulse. Following a discharge, V is immediately reset to V_0.

When $V_\infty>S_0$, the LIFM discharges periodically, even in the absence of inputs. In this respect, its dynamics in the presence of periodic modulation and additive noise resemble those of the perfect integrator that have been thoroughly analyzed in [12]. In the following, we assume that $V_\infty<S_0$, so that in the absence of inputs, the membrane potential settles at V_∞, and there are no discharges.

When the input is a sinusoidal current $I(t)=I_0+I_1\sin(\Omega t+\theta)$, the solution of Eq. (2.1) is given by

$$V_{\mathrm{mod}}(t)=V_0e^{-(t-t')/\tau}+\mu\tau(1-e^{-(t-t')/\tau}) + \frac{A\tau}{\sqrt{1+(\Omega\tau)^2}}[\sin(\Omega t+\theta-\varphi) - e^{-(t-t')/\tau}\sin(\theta-\varphi)], \tag{2.2}$$

where $\tau=RC$ is the membrane time constant, $\mu=(V_\infty/\tau)+(I_0/C)$, $\varphi=\arctan(\Omega\tau)$, t' $(\leqslant t)$ is the last time the unit fired, and $A=I_1/C$. We refer to A as the modulation amplitude, and denote by $T=2\pi/\Omega$ the modulation period. Depending on the values of these two parameters, the input is either subthreshold or suprathreshold. When the amplitude is large enough to generate firing, the stimulus is referred to as suprathreshold. Conversely, subthreshold modulation refers to the case where A is small, so that the LIFM does not display sustained firing. In the following, we deal only with subthreshold inputs. The various responses of the deterministic LIFM to sinusoidal stimulation have been described in [13].

B. Stochastic model

When a neuron receives infinitesimally small excitatory and inhibitory inputs via corresponding synaptic connections, subthreshold dynamics of the membrane potential can be described as follows (for reviews, see [14]):

$$dV(t)=\left(-\frac{V}{\tau}+\mu\right)dt+\sqrt{2D}dW(t), \quad V(t)<S_0 \tag{2.3}$$

where D represents the intensity of the input noise and $W(t)$ the standard Wiener process. $V(t)$ is an Ornstein-Uhlenbeck (OU) stochastic process.

In the presence of a sinusoidal input, Eq. (2.3) becomes

$$dV(t)=\left[-\frac{V}{\tau}+\mu+A\sin(\Omega t+\theta)\right]dt+\sqrt{2D}dW(t), \quad V(0)=V_0, \quad V(t)<S_0. \tag{2.4}$$

V is no longer an OU process. However, using V_{mod} of Eq. (2.2), we can change variables according to

$$X(t)=V(t)-V_{\mathrm{mod}}(t), \quad S_{\mathrm{mod}}(t)=S_0-V_{\mathrm{mod}}(t). \tag{2.5}$$

Thus, Eq. (2.4) is transformed into

$$dX(t)=-\frac{X}{\tau}dt+\sqrt{2D}dW(t), \quad X(0)=0, \quad X(t)<S_{\mathrm{mod}}(t). \tag{2.6}$$

Equation (2.6) shows that the transformed variable $X(t)$ is an OU process. In other words, the periodically modulated LIFM with constant threshold is equivalent to the LIFM without membrane modulation but with an appropriately time-dependent threshold. This is illustrated in Fig. 1, which shows the behavior of the original membrane potential (upper panel) together with the transformed one (lower panel). The advantage of this transformation is that the discharge

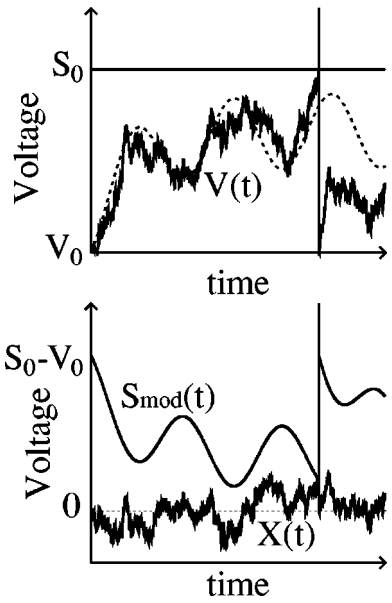

FIG. 1. Schematic transformation of the variables. Upper panel corresponds to Eq. (2.4) and lower panel to Eq. (2.6). Dotted curve in upper panel is the membrane potential without noise, corresponding to $V_{\mathrm{mod}}(t)$ in Eq. (2.2). Abscissae: time in arbitrary units; ordinates: voltage in arbitrary units.

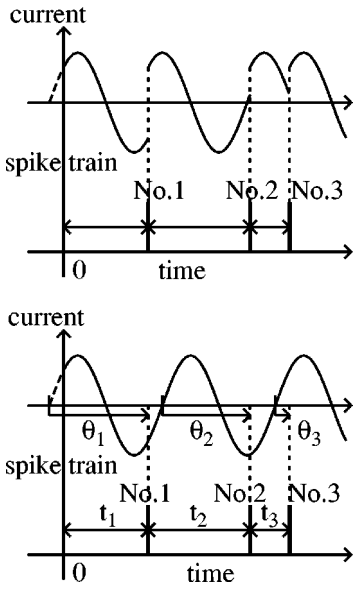

FIG. 2. Schematic spike train and corresponding current for both endogenous (upper panel) and exogenous signal (lower panel). For the exogenous signal, the phase of the input current is not reset after each firing. The phase θ_n of the input at nth firing and the interspike interval t_n between $(n-1)$th and nth firing are random variables, and they have corresponding probability density function, $h_n(\theta)$ and $i_n(t)$, respectively. Abscissae: time in arbitrary units; ordinates of the current: in arbitrary units; ordinates of the spike train: voltage in arbitrary units.

times of the model can be derived from the first-passage time of an OU process through a smooth boundary. This is detailed in the following.

The time t at which X reaches S_{mod} for the first time given $X(0)=0$ is called the first-passage time (t_{FP}):

$$t_{\mathrm{FP}}=\inf\{t:X(t)>S_{\mathrm{mod}}(t)|X(0)=0<S_{\mathrm{mod}}(0)\}. \quad (2.7)$$

t_{FP} is a random variable with probability density function (PDF) $g(S_{\mathrm{mod}}(t),t|\theta)$ satisfying the following equation [14]:

$$p(x,t|0,0)=\int_0^t g(S_{\mathrm{mod}}(\tau),\tau|\theta) \times p(x,t|S_{\mathrm{mod}}(\tau),\tau)d\tau \quad (x>S_{\mathrm{mod}}(t),\ S_{\mathrm{mod}}(0)>0), \quad (2.8)$$

where $p(x,t|y,s)$ is the transition PDF of the process $X(t)$ and satisfies the Fokker-Planck equation [14]:

$$\frac{\partial p}{\partial t}=-\frac{\partial}{\partial x}\left[-\frac{x}{\tau}p\right]+D\frac{\partial^2 p}{\partial x^2}. \quad (2.9)$$

The solution $p(x,t|y,s)$ of Eq. (2.9) is given by

$$p(x,t|y,s)=\frac{1}{\sqrt{2\pi}\sigma_{t,s}}\exp\left[-\frac{(x-ye^{-(t-s)/\tau})^2}{2\sigma_{t,s}^2}\right], \quad (2.10)$$

$$\sigma_{t,s}^2=2D\tau(1-e^{-2(t-s)/\tau}). \quad (2.11)$$

Equation (2.8) is a Volterra integral equation of the first type with respect to g, which cannot be solved analytically except for some special boundaries $S_{\mathrm{mod}}(t)$. A special attention should be paid for numerical computation of the solution, because the function $p(x,t|S_{\mathrm{mod}}(\tau),\tau)$ is singular as $\tau\to t$. Giorno *et al.* [15] proposed a numerical procedure for solving Eq. (2.8) for a smooth time-dependent boundary. We used the method in order to perform the numerical computation for the t_{FP} PDF.

III. COMPUTATION OF THE ISI DISTRIBUTION

Following [11], we classify inputs as endogenous and exogenous depending on whether the input phase is reset to a fixed value after each discharge or not. To our knowledge, previous studies have mainly dealt with the endogenous modulation. In the following two subsections, we describe both cases successively and propose numerical methods to calculate the interspike interval PDF for each of them.

A. Endogenous periodicity

When the input phase is reset to a fixed value after each discharge (upper panel Fig. 2), the ISI distribution is given by the t_{FP} PDF. This distribution depends on the initial phase θ as illustrated in Fig. 3. Usually, θ is taken as $\pi/2$ because, for this value, the ISI distribution is close to that of the corresponding exogenous forcing, in the sense that the peaks of the ISI distribution are situated close to the multiples of the modulation period. Hence, for the endogenous periodic signal, we describe the ISI distribution as $g(t|\pi/2)$.

B. Exogenous periodicity

When the periodic signal is exogenous, the membrane potential and the threshold are reset after the discharge but not the phase of the external input (lower panel Fig. 2).

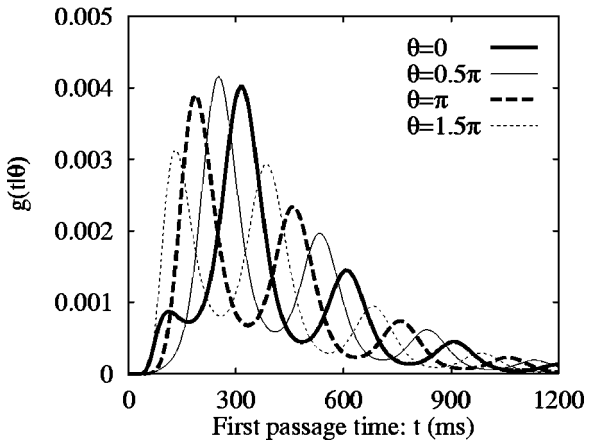

FIG. 3. First passage time probability density function $g(t|\theta)$ for four different initial phases $\theta=0$ rad, $\pi/2$ rad, π rad, and 2π rad. Abscissa: first passage time in milliseconds; ordinate: probability density in kilohertz. Parameters: $\mu=0.1$ V/s, $A=0.05$ V/s, $\tau=1/0.006$ ms (we chose these values to compare our results with those of Bulsara *et al.* in [9]), $T=300$ ms, $S_0=20$ mV, $D=0.2$ (mV)^2, $V_0=0$ mV.

Hence, the phase of the signal at the firing is a random variable. In this subsection, we propose a method to calculate the PDF of this variable and derive the ISI distribution from it.

The initial phase θ completely determines the time course of the boundary $S_{\mathrm{mod}}(t)$ in the t_{FP} PDF $g(S_{\mathrm{mod}}(t),t|0)$ defined by Eq. (2.8). Hence, we denote the PDF by $g(t|\theta)$ for the sake of convenience. Also let us denote

$$f(\phi|\theta)=\frac{1}{\Omega}\sum_{k=0}^{\infty} g\left(kT+\frac{\phi-\theta}{\Omega}\middle|\theta\right), \tag{3.1}$$

where $g(t|\theta)=0$ if $t<0$. Convergence of this series is ensured by the fact that for large t, g can be bounded by exponentials [16]. The function $f(\phi|\theta)$ is the PDF of the next firing phase ϕ given the last discharge phase θ, and satisfies $\int_0^{2\pi} f(\phi|\theta)d\phi=1$, $f(\phi|\theta)>0$.

Let $h_n(\theta)(0\leqslant\theta<2\pi)$ be the PDF of the phase at the time of nth firing, $n=1,2,\ldots$. Then, $h_n(\phi)$ is obtained by the following equation:

$$\begin{aligned} h_n(\phi)&=\int_0^{2\pi} f(\phi|\theta)h_{n-1}(\theta)d\theta, \quad n=1,2,\ldots \\ &\equiv \mathcal{P}h_{n-1}(\phi), \end{aligned} \tag{3.2}$$

where $h_0(\theta)$ is the PDF of the initial phase θ_0 and satisfies $h_0(\theta)>0$, $\int_0^{2\pi} h_0(\theta)d\theta=1$. We call $\mathcal{P}$ the stochastic phase transition operator (SPTO). It is a Markov operator with kernel $f(\phi|\theta)$. A similar operator was used in the analysis of stochastic phase locking [17] and linearization by noise [18]. Figure 4 shows examples of $f(\phi|\theta)$ for four different noise intensities D.

Applying the SPTO iteratively to the PDF h_0 of the initial phase, we can obtain h_n as

$$h_n=\mathcal{P}h_{n-1}=\mathcal{P}(\mathcal{P}h_{n-2})=\cdots=\mathcal{P}^n h_0. \tag{3.3}$$

Since

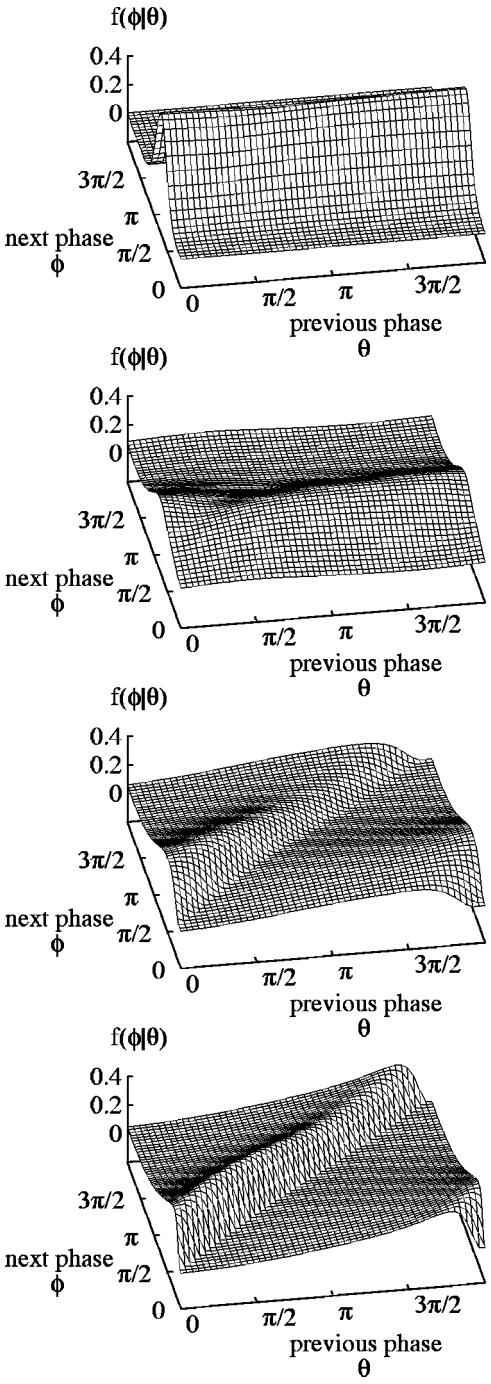

FIG. 4. The kernel $f(\phi|\theta)$ of the SPTO $\mathcal{P}$ for different noise intensities, $D=0.02$ (mV)^2 (upper panel), 0.2 (mV)^2 (second panel from top), 1 (mV)^2 (third panel from top), and 2 (mV)^2 (lower panel). Axis of θ: the phase of the input at the previous firing, in radians. Axis of ϕ: the phase of the input at the next firing, in radians. Axis of $f(\phi|\theta)$: the probability density function of the next firing phase ϕ given the previous firing phase is θ, in kilohertz. Parameters: $\mu=0.1$ V/s, $A=0.05$ V/s, $\tau=1/0.006$ ms, $T=300$ ms, $S_0=20$ mV, $V_0=0$ mV.

$$\int_0^{2\pi} \inf_{\theta} f(\phi|\theta)d\phi>0, \tag{3.4}$$

$\{\mathcal{P}^n\}$ is asymptotically stable [19], that is, there exists a unique density function h_∞ such that $\mathcal{P}h_\infty=h_\infty$ and

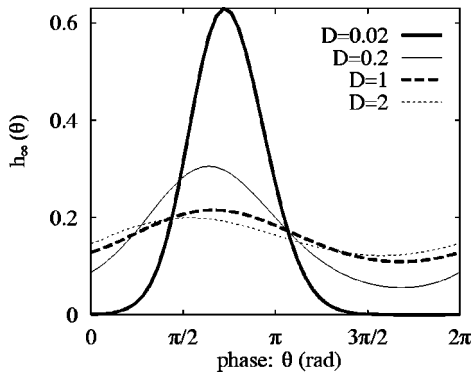

FIG. 5. Phase distribution $h_\infty(\theta)$ for $D=0.02$ $(\mathrm{mV})^2$, 0.2 $(\mathrm{mV})^2$, 1 $(\mathrm{mV})^2$, and 2 $(\mathrm{mV})^2$. Abscissa: the phase θ of the input at the firing, in radians; ordinate: probability density in $(\mathrm{radian})^{-1}$. Parameters: $\mu=0.1$ V/s, $A=0.05$ V/s, $\tau=1/0.006$ ms, $T=300$ ms, $S_0=20$ mV, $V_0=0$ mV.

$$\lim_{n\to\infty}||\mathcal{P}^n h_0 - h_\infty||=0 \quad \text{for every} \quad h_0. \tag{3.5}$$

We refer to $h_\infty(\theta)$ as phase distribution. It corresponds to the normalized cycle histogram used by neurophysiologists to analyze experimental data. Figure 5 shows h_∞ for four different values of D.

The PDF of the time interval t_n between $(n-1)$th and nth spikes, $i_n(t)$, is given by

$$i_n(t)=\int_0^{2\pi} g(t|\theta)h_{n-1}(\theta)d\theta, \quad n=1,2,\ldots \tag{3.6}$$

and $i_\infty(t)$, the ISI distribution, satisfies

$$i_\infty(t)=\int_0^{2\pi} g(t|\theta)h_\infty(\theta)d\theta. \tag{3.7}$$

Throughout this work, we computed h_∞ by iterating $\mathcal{P}$ and then obtained i_∞ using Eq. (3.7). Comments for numerical calculation are provided in the Appendix.

In order to allow a better comparison with prior studies, results shown in the figures were all computed with the same parameters as [9]. We also performed similar numerical investigations with other parameter sets, including those of [10]. But, these are not illustrated through the figures, as the main conclusions remain unchanged.

IV. TIME-SCALE MATCHING IN TIME DOMAIN

Bulsara *et al.* [9] showed that, for the LIFM receiving subthreshold periodic modulation, the height of the ISI distribution at the modulation period goes through a maximum with increasing D, indicating that noise of intermediate amplitude can improve signal transmission. They observed that the same quantity also goes through a maximum with increasing T. They showed that at both maxima, the time scale of the noise-induced firing matched the modulation period, in the sense that (1) in the former case where T was fixed and D varied, the mode $t_m(D^*)$ of the ISI distribution in the absence of modulation (i.e., $A=0$) satisfied $t_m(D^*)\simeq T$ at the optimal noise level D^*, (2) while in the latter case, where D was fixed and T varied, the optimal modulation period T^* satisfied $T^*\simeq t_m(D)$, where D^* (or T^*) is the optimal value which gives the hump of the height of the ISI distribution at T while varying D (or T) for fixed T (or D).

In this section, we examine consecutively the influence of the input amplitude on these two conditions. For each we consider both situations where the periodic signal is endogenous and exogenous.

A. For fixed D

Let us start with the time-scale matching that takes place when the modulation period T is varied, while the noise amplitude D is kept constant. For an endogenous signal, the ISI distribution is $g(t|\pi/2)$ as mentioned before. Figure 6 (upper panel) is an example of the ISI distribution for four different T. The abscissa is normalized by the modulation period to facilitate the comparison. For small T (thick solid line), the ISI distribution displays several peaks which are close to multiples of T (not all are shown). This is a signature of skipping: discharges occur mainly at a given phase, but not necessarily at every period. For short periods, the peak at T is smaller because the LIFM does not have time to recover from the refractory period within one stimulation period. As T increases, so does the height of the ISI distribution peak at T. At the same time, a new peak at a shorter time appears. This peak is due to the fact that, for slow modulation, the LIFM generates a burst of tightly packed spikes every time the input approaches its maximal value. Therefore the discharge train is a succession of bursts separated by intervals close to the modulation period. The intraburst ISIs are close to the refractory period. The number of discharges within each burst varies from one burst to another, but steadily increases with the period. This lengthening of the burst explains the increase of the size of the first peak in the ISI distribution, as the peak height at T progressively decreases. Overall, this leads to the hump shaped dependence of $g(T)$ on T illustrated in Fig. 6 (third panel from top). Similar humps exist for $g(kT)$, i.e., at multiples of the modulation period. These are shown in the three-dimensional (3D) representation of the ISI distribution as a function of both the ISI duration and the period T in Fig. 7 (upper panel).

When the input is exogenous, i.e., its phase is not reset, the overall dependence of the ISI distribution on T is the same. Figure 6 (second and fourth panels from top) and Fig. 7 (lower panel) illustrate this. The notable difference is that the peaks in the ISI are less marked for the exogenous signal. This results from the fact that the phase distribution has a nonzero width. This difference leads to a smaller optimal period T^* [275 ms against 300 ms in Fig. 6 (second and fourth panels from top)].

Perfect time-scale matching occurs when T^* is equal to the mode t_m of the ISI distribution *without* modulation for fixed D, that is,

$$T^*=t_m(D) \text{ for fixed } D \text{ while changing } T, \tag{4.1}$$

where T^* is the optimal value of T that maximizes the peak of the ISI distribution at T [i.e., $g(T)$ or $i_\infty(T)$ for endogenous and exogenous forcing, respectively]. Figure 8 (upper panel) shows $t_m(D)$ versus T^* for several modulation amplitudes A, that is to say, for each value of D, the optimal period T^* is plotted against $t_m(D)$. The graph for $A=0.1$ is

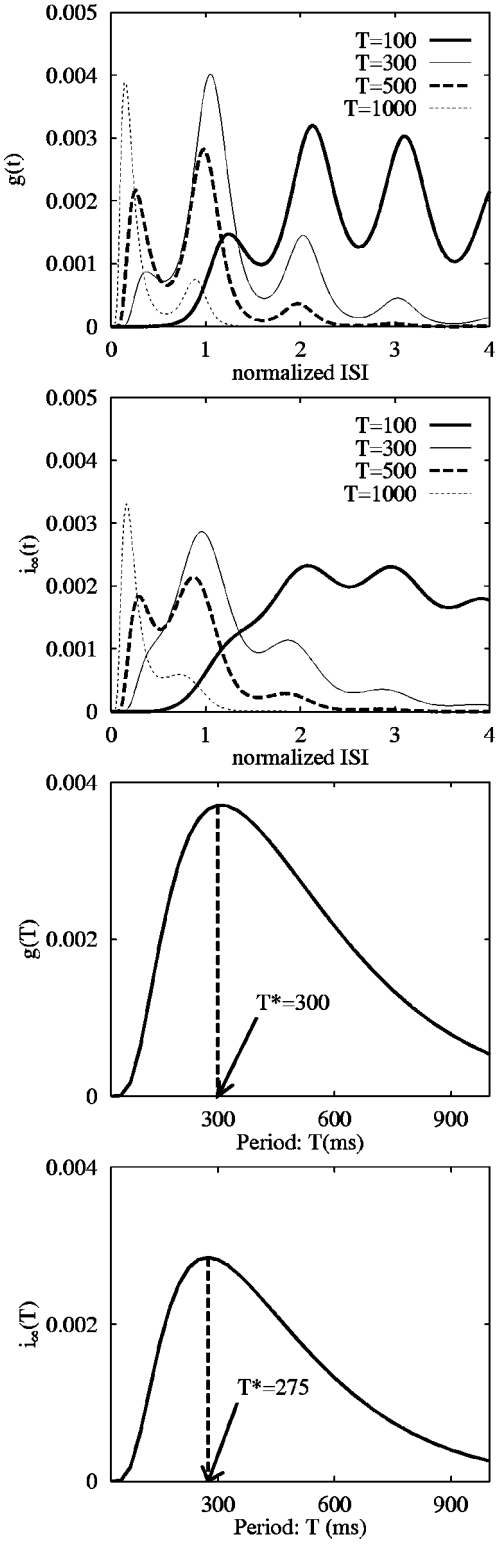

FIG. 6. Two upper panels: ISI distribution for endogenous (upper panel) and exogenous (second panel from top) signals for four different modulation periods T. Abscissae: ISI normalized by the period T (dimensionless); ordinates: probability density in kilohertz. Two lower panels: the height of the ISI distribution at T for endogenous (third panel from top) and exogenous (lower panel) signals. T^* represents the optimal period that maximizes the height of the ISI distribution at T. Abscissae: the period T in milliseconds; ordinates: probability density in kilohertz. Parameters: $\mu=0.1$ V/s, $\tau=1/0.006$ ms, $S_0=20$ mV, $V_0=0$ mV, $D=0.2$ $(\mathrm{mV})^2$, and $A=0.05$ V/s.

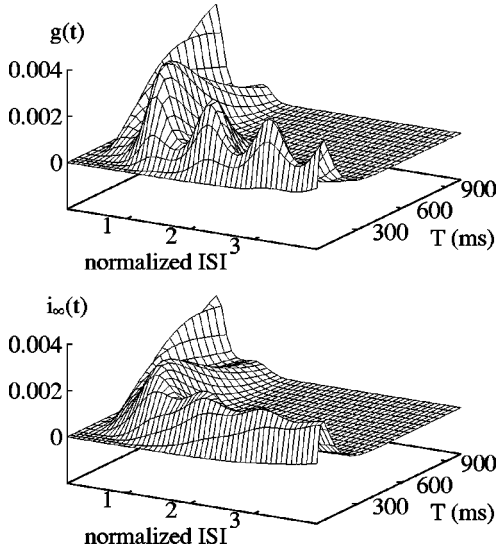

FIG. 7. Three-dimensional representations of the ISI distribution (in kilohertz) as a function of the normalized ISI (dimensionless) and the period T in milliseconds for endogenous (upper panel) and exogenous (lower panel). The parameters are the same as in Fig. 6.

interrupted about $T^*=200$ ms. This is because larger periods lead to suprathreshold modulation. Equation (4.1), which characterizes time-scale matching, corresponds to the diagonal. This holds for $A=0$, but not for larger values of A, the graphs of T^* move away from the perfect matching. The fact that the curve is on the diagonal for $A=0$ stems from the definition of T^*.

As A is increased the curves depart from the perfect matching, showing that T^* is larger than $t_m(D)$. This influence of the modulation amplitude is independent of the resetting strategy as attested by the similarity between the two upper panels in Fig. 8 showing, respectively, the endogenous and the exogenous cases.

The fact that time-scale matching deteriorates for large amplitudes and T^* suggests that this may be due to the dependence of membrane potential oscillation amplitude on the modulation period. To account for this effect, we adjusted the value of A, the modulation amplitude, so as to keep the value of $A'=\tau A/\sqrt{1+(\Omega\tau)^2}$, the effective oscillation amplitude, constant while T was tuned to obtain maximal response. In this way, for each value of the noise amplitude D and effective modulation amplitude A', we obtained a new optimal period T^* that maximized the ISI distribution at T. The two lower panels in Fig. 8 show the graphs for $t_m(D)$ versus T^* for endogenous and exogenous periodic stimulation. In the former, perfect time-scale matching is achieved for all effective amplitudes, as all curves are superimposed on the diagonal. In the latter, the same holds for low A'. However, at larger A', the optimal period T^* is smaller than $t_m(D)$. This effect is more pronounced at large $t_m(D)$, i.e., low noise levels.

Bulsara *et al.* proposed an approximate t_{FP} PDF using the method of images. The two upper panels of Fig. 9 show time-scale matching using their expression [Eq. (16) in [9]] for the ISI distribution of endogenous periodic signal. Comparison of these results to Fig. 8 (first and third panels from top) shows that the main properties of the time-scale matching are preserved under this approximation. For instance, the

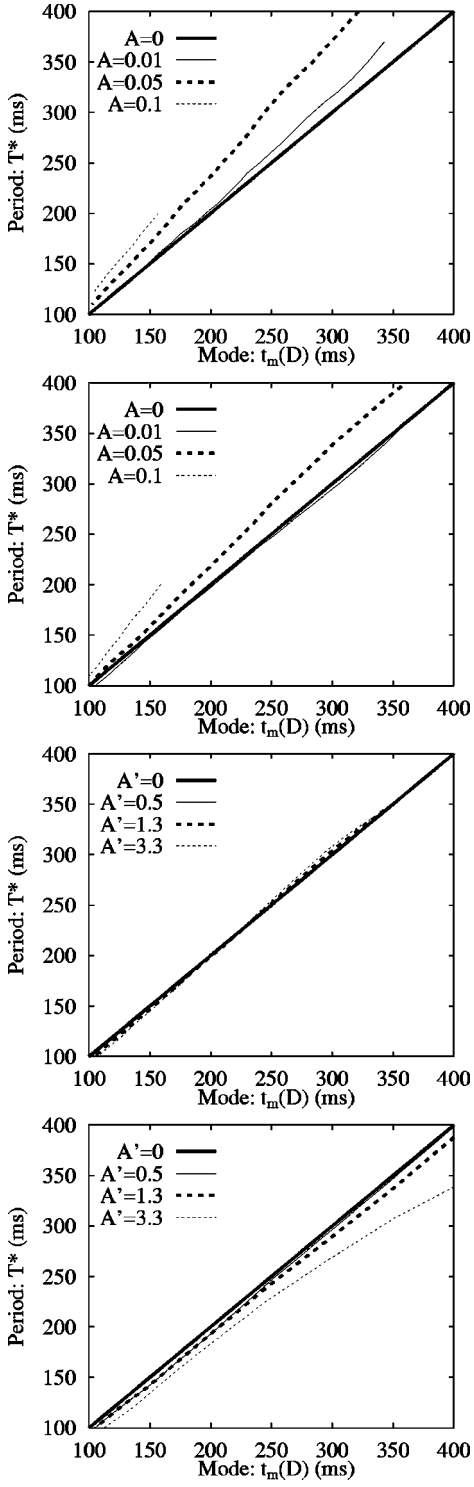

FIG. 8. Time-scale matching for fixed D. The optimal period T^* that maximizes the height of the ISI distribution at the modulation period T for a given value of D is represented against the mode $t_m(D)$ of the ISI distribution in the absence of modulation. First and third panels from top correspond to the endogenous signals while second and fourth panels from top are those of exogenous signals. The graphs in the two upper panels show T^* for four different values of A, those in the two lower panels show the same quantity for four different values of $A' = A\tau/\sqrt{1+(\Omega\tau)^2}$. Abscissae: the mode $t_m(D)$ of the ISI distribution without modulation in milliseconds. Large t_m corresponds to low noise intensity. Ordinates: the optimal value T^* in milliseconds. All parameters except D and A are the same as in Fig. 6.

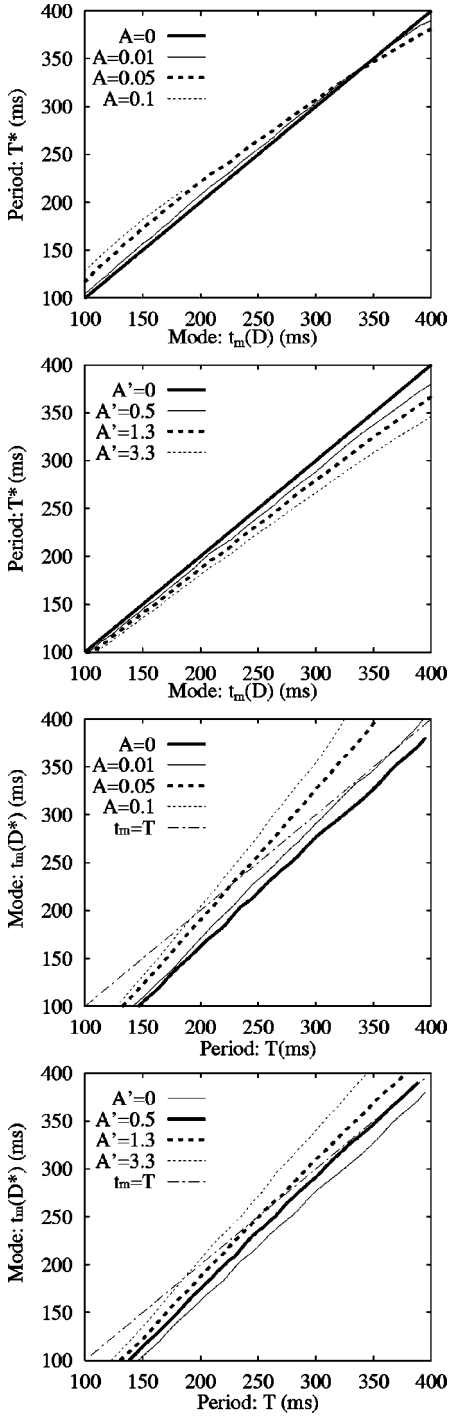

FIG. 9. Time-scale matching calculated by the method of the images [9]. Periodic signal is considered as endogenous, so the ISI distribution is $g(t|\pi/2)$. Two upper panels: abscissae: the mode $t_m(D)$ of $g(t|\pi/2)$ without modulation, in milliseconds; ordinates: the optimal value T^* in milliseconds, which gives a maximum of $g(T|\pi/2)$ while changing T for fixed D. We plot how T^* changes while varying $t_m(D)$ (i.e., D) for fixed A in upper panel and $A' = A\tau/\sqrt{1+(\Omega\tau)^2}$ in the second panel from top. Two lower panels: Abscissae: T in milliseconds; ordinates: the mode $t_m(D^*)$ of the ISI distribution without modulation, in milliseconds. D^* is the noise intensity which gives a maximum of $g(T|\pi/w)$ while changing D for fixed T. We plot how $t_m(D^*)$ (i.e., D^*) changes while varying T for fixed A in third panel from top and $A' = A\tau/\sqrt{1+(\Omega\tau)^2}$ in lower panel. Parameters: $\mu = 0.1$ V/s, $\tau = 1/0.006$ ms, $S_0 = 20$ mV, $V_0 = 0$ mV.

graphs for fixed A' are close to parallel lines, and move away from the diagonal line with increasing A or A'. Furthermore, the directions of the changes are similar to those for Fig. 8 except in the upper panel of Fig. 9 at low noise levels, where the approximation underestimates the value of T^*.

B. For fixed T

The previous results were concerned with the matching for a given D as T is changed. Here, we consider the converse situation whereby T is kept constant while D is varied. Interestingly, the qualitative changes that take place in the ISI distribution as the noise intensity D is increased are similar to those described in the preceding section when T was increased. As shown in the two upper panels of Fig. 10 for both endogenous and exogenous forcing, low noise levels are associated with skipping with peaks at multiples of the modulation period. As the noise level is increased the peak at T first grows and then decays as the noise-dominated firing with short intervals takes over. The two lower panels in Fig. 10 illustrate the respective graphs of the ISI distribution at T as the noise is increased. Again both curves are hump shaped with the exogenous signal evoking the smaller maximum value. The corresponding optimal noise levels D^* are close to one another. The fact that the responses at multiples of T also go through maxima as D is increased can be seen in the three-dimensional representations in Fig. 11. These results together with the similar description given in the preceding section corroborate the findings in [9], and show that phase resetting does not introduce important changes in the response of the system.

Similarly to the preceding section, we examine whether at the optimal noise levels that maximize the response of the system there is a matching between the time scales. Let us denote by D^* the optimal noise amplitude which maximizes $g(T|\pi/2)$ or $i_\infty(T)$, and by $t_m(D^*)$ the mode of the corresponding ISI distribution in the absence of modulation. Time-scale matching occurs when we have the relation

$$t_m(D^*)=T \quad \text{for fixed} \quad T \ \text{while changing} \ D. \quad (4.2)$$

The two upper panels in Fig. 12 show the graphs of T versus $t_m(D^*)$ for several modulation amplitudes for endogenous and exogenous forcing, respectively. The graph for $A=0$ is far from the diagonal line. Therefore Eq. (4.2) is not satisfied for $A=0$ or for small A because the ISI distribution at T [i.e., $g(T)$ or $i_\infty(T)$] varies continuously with A. In other words, for this range of A, the mode t_m of the ISI distribution for $D=D^*$ is not equal to T. The reason for this is that at very weak modulation amplitudes, the periodicity of the input is not reflected in the ISI distribution, i.e., there are no marked peaks at the multiples of T. Therefore the value of the ISI distribution at T is not in the vicinity of a clearly defined local maximum. For a given signal amplitude A, the situation improves at large T because the corresponding effective amplitude A' is large, so that the periodicity of the input affects the discharge pattern. For the same reason, the curves approach the diagonal as A is increased: the optimal noise level moves closer to the perfect matching condition. When the modulation amplitude A is adjusted to account for the dependence of A' on T, the distance between the graph of t_m as a function of T and the diagonal varies less with T even though there is still a slight improvement at larger T. The line for each level of A' runs almost parallel to the diagonal. However, unlike Fig. 8 (third panel from top), these are not su-

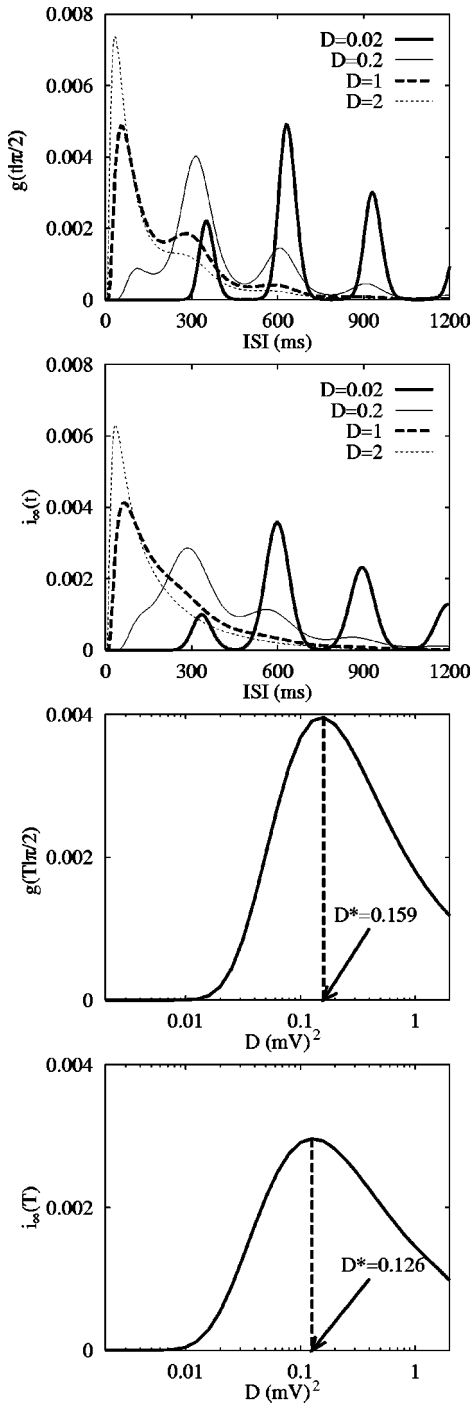

FIG. 10. Two upper panels: ISI distribution for endogenous (upper panel) and exogenous (second panel from top) signals for four different noise intensities D. Abscissae: ISI in milliseconds; ordinates: probability density in kilohertz. Two lower panels: the height of the ISI distribution at T for endogenous (third panel from top) and exogenous (lower panel) signals. D^* represents the optimal noise that maximizes the height of the ISI distribution at T. Abscissae: the noise intensity D in $(\text{millivolts})^2$; ordinates: probability density in kilohertz. Parameters: $\mu=0.1$ V/s, $\tau=1/0.006$ ms, $S_0=20$ mV, $V_0=0$ mV, $T=300$ ms, and $A=0.05$ V/s.

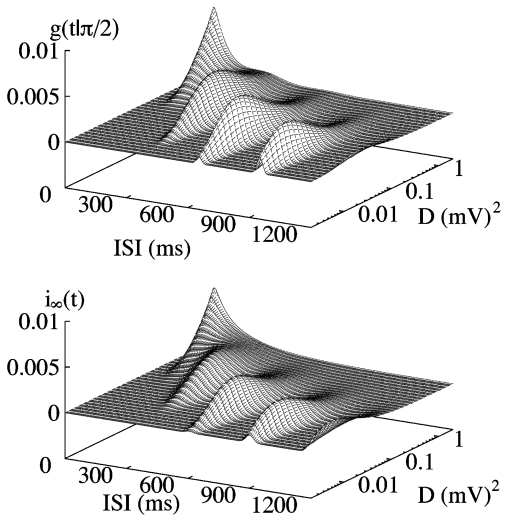

FIG. 11. Three-dimensional representations of the ISI distribution (in kilohertz) as a function of ISI in milliseconds and noise intensity D in (millivolts)^2 for endogenous (upper panel) and exogenous (lower panel). The parameters are the same as in Fig. 10.

perimposed. As expected, the distance between the lines and the diagonal is smaller at larger A'. With increasing A', the distance between the membrane potential V at T and the threshold S decreases. Consequently, D^* decreases and $t_m(D^*)$ increases. Hence, the graph moves towards the diagonal line with increasing A'.

The two lower panels of Fig. 9 show that the method of images captures well the discrepancy between the perfect matching and the actual value of $t_m(D^*)$ at low amplitudes, and the progressive movement of the lines towards the diagonal as the amplitude or the period are increased. Here again, compared to Fig. 12 (first and third panels from top), this approximation overestimates the value of $t_m(D^*)$ (i.e., underestimates D^*) at large modulation periods and amplitudes.

V. TIME-SCALE MATCHING IN FREQUENCY DOMAIN

Following [9,10], we assume that the signal is endogenous, that is, the phase of the sinusoidal signal is reset to the same value θ_0 after each discharge. Hence, the discharge times of the model form a renewal point process, i.e., they are independent and identically distributed. This allows us to compute the power spectral density of the spike train from the ISI distribution according to [10,12]

$$P(\omega)=\frac{1}{\pi\langle t\rangle}\left(1+\frac{\tilde{g}(\omega)}{1-\tilde{g}(\omega)}+\frac{\tilde{g}(-\omega)}{1-\tilde{g}(-\omega)}\right), \qquad (5.1)$$

where $\langle t\rangle$ is the mean t_{FP} and

$$\tilde{g}(\omega)=\int_0^\infty g(t)\exp[i\omega t]dt.$$

For large ω, the PSD stabilizes at $1/(\pi\langle t\rangle)$. Additionally, when the spike train is the Poisson impulse noise with parameter $1/\langle t\rangle$, the PSD is flat and equal to $1/(\pi\langle t\rangle)$ for all ω. This suggests that considering the quantity F(ω)

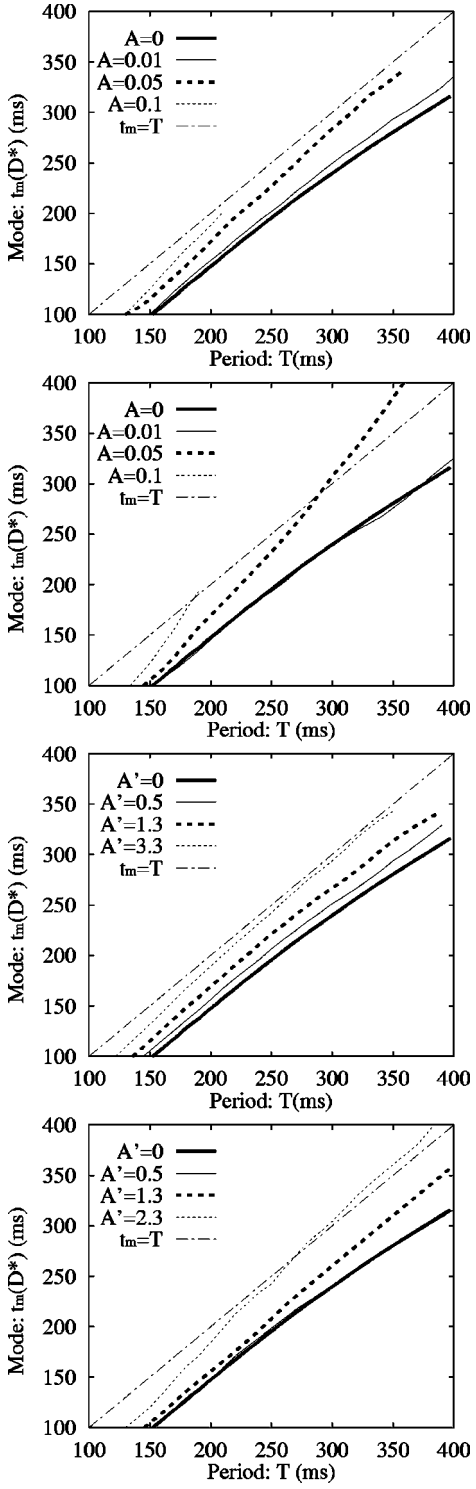

FIG. 12. Time-scale matching for fixed T. $t_m(D^*)$ (the mode of the ISI distribution without modulation at the optimal noise D^* that maximizes the height of the ISI distribution at the modulation period T) is represented against the period T. First and third panels from top correspond to the endogenous signals while second and fourth panels from top are those of exogenous signals. The graphs in the two upper panels show $t_m(D^*)$ for four different values of A, those in the two lower panels show the same quantity for four different values of $A'=A\tau/\sqrt{1+(\Omega\tau)^2}$. Abscissae: the period T in millisecond; ordinates: the mode $t_m(D^*)$ of the ISI distribution without modulation in milliseconds. All parameters except T and A are the same as in Fig. 10.

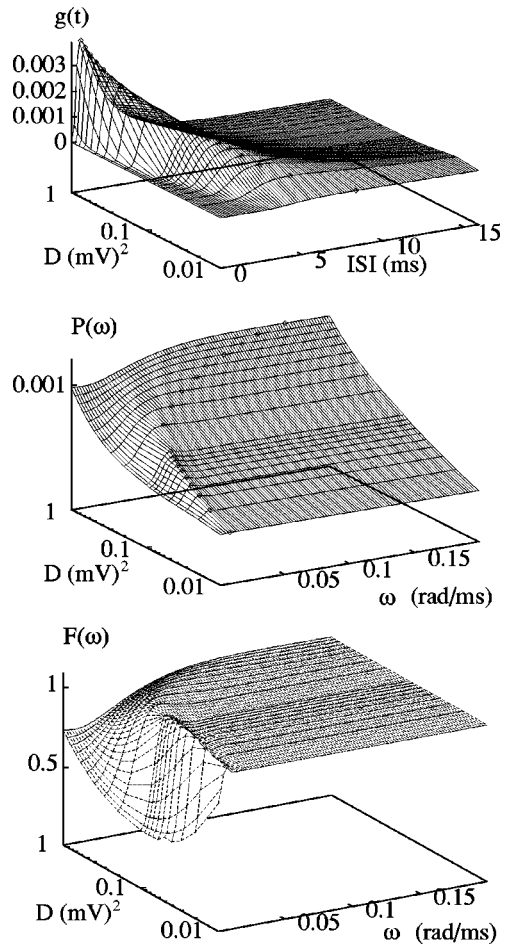

FIG. 13. Three-dimensional representations of the ISI distribution $g(t|\pi/2)$ in kilohertz (upper panel), the PSD $P(\omega)$ in kilohertz (second panel from top) and $F(\omega)$ (dimensionless) (lower panel) in the absence of the modulation. Axes of ISI in upper panel: the ISI in milliseconds. Axes of D in all panels: the noise intensity in (millivolts)^2. Axes of ω in the two lower panels: the angular frequency of the periodic stimulation current in radians per millisecond. Parameters: $\mu=0.1$ V/s, $\tau=1/0.006$ ms, $S_0=20$ mV, $V_0=0$ mV, $A=0$ V/s.

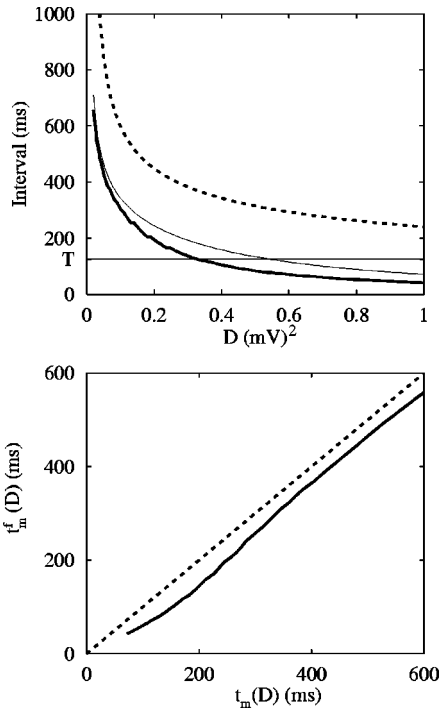

FIG. 14. Upper panel: noise intensity D in (millivolts)^2 versus the mode t_m (thin solid line) of the ISI distribution and the mean t_M (dotted line) together with $t_m^f=2\pi/\omega_m^f$ (thick solid line), where ω_m^f is the mode of the PSD, or equivalently that of F. We drew a horizontal line at $T=2\pi/0.05$, which is often used as modulation period in our results. Lower panel: the relation between t_m and t_m^f. Units of both axes in lower panel are milliseconds. Parameters: $S=20$ mV, $\tau=1/0.006$ ms, $\mu=0.1$ V/s, $V_0=0$ mV, $A=0$ V/s.

$=\pi\langle t\rangle P(\omega)$ can be advantageous for the comparison of the discharge patterns at various noise levels in the frequency domain [10].

Figure 13 shows the ISI distribution and corresponding $P(\omega)$ as well as $F(\omega)$ as a function of noise intensity D in the absence of periodic input. As the noise level is increased, shorter intervals become more likely, and the mode of the ISI distribution moves to the left. In the same way, the mode of the PSD (and consequently that of F) moves right, showing the increase in high frequencies.

In the time domain, we considered the mode of the ISI distribution in the absence of modulation as the appropriate time scale of the spontaneous firing. This choice followed the results in [9] that showed that with this quantity, time-scale matching could occur when the response of the LIFM was maximal. The upper panel of Fig. 14 illustrates three possible candidates for the noise-induced firing time scale in the frequency domain, namely, the mode t_m (thin solid line) of the ISI distribution and the mean t_M (dotted line) together with $t_m^f=2\pi/\omega_m^f$ (thick solid line), where ω_m^f is the mode of the PSD, or equivalently that of F. There is a significant difference between these quantities and we have $t_m^f<t_m<t_M$. The lower panel of Fig. 14 shows the relation between the mode t_m in time domain and the mode t_m^f in frequency domain. In the following, we assume that the appropriate time scale in the frequency domain is t_m^f. Not only does this choice seem natural in the frequency domain, but also, it is the one that led to better matchings in all conditions. Furthermore, even in cases where time-scale matching was not achieved, t_m^f was the closest of the three to the modulation period.

To assess the periodicity of the spike train in the frequency domain, we evaluated the peaks of the PSD and F near Ω, and examined how these changed when either the modulation period or the noise were varied. The maximal value of F near Ω is also referred to as the signal-to-noise ratio (SNR) [10]. The two quantities are defined as

$$P_M=\max\{P(\omega)|0.93\Omega<\omega<1.07\Omega\}, \tag{5.2}$$

$$S=\max\{F(\omega)|0.93\Omega<\omega<1.07\Omega\}=\pi\langle t\rangle P_M. \tag{5.3}$$

SNR compares the value of the maximum of the PSD at the modulation frequency to its base level $1/(\pi\langle t\rangle)$ at large frequencies. However, as $\langle t\rangle$ varies when either the modulation

period T or the noise intensity D is modified, P_M and SNR are not proportional when plotted against one of these parameters. Yet, practically, we observed that $\langle t \rangle$ varies little with T in the range of parameters that we considered, so that F and PSDs are almost proportional when T was varied for fixed D.

A. For fixed D

At first, we examine how the two quantities P_M and SNR change, when, for a fixed D, the modulation period T is varied. To our knowledge, previous studies have not determined whether this situation leads to a ''resonancelike'' phenomenon. As our aim is mainly to determine whether P_M and SNR have a maximum when the modulation period is near t_m^f, we limit our investigation to periods in the vicinity of this value.

The left column in Fig. 15 shows how the ISI distributions for three different modulation periods vary when the input amplitude is increased from $A=0$ to $A=0.05$. The abscissae have been normalized by the modulation period to facilitate the comparison between the different curves. The middle column in the same figure represents the corresponding function F. The PSD is not shown since, as mentioned before, $\langle t \rangle$ varies little with T so that there is little difference between PSD and F. For $A \neq 0$, F displays a maximum at the modulation frequency. The larger the modulation amplitude, the larger the corresponding peak in F. As the period is increased, the peak height, i.e., the SNR, goes through a maximum. The right column shows the variation of the peak height as a function of t_m^f/T. Time-scale matching occurs when the mode of the SNR coincides with one. This condition is satisfied at $A=0$, as a consequence of the definition of t_m^f. It still holds approximately for small modulation amplitudes (second panel from top in right column of Fig. 15). However, at larger modulations, the mode of the SNR moves to values smaller than one. In other words, the SNR is maximal at periods larger than t_m^f.

The upper panel of Fig. 16 shows how the SNR changes progressively with the input amplitude (the noise level is different from that in Fig. 15). The arrow indicates $t_m^f(D)$, i.e., when the mode is situated at this point, there is perfect matching. The difference between the optimal modulation period and the value that would lead to perfect matching can also be seen in the lower panel of Fig. 16, which shows $t_m^f(D)$ versus T^* for various input amplitudes. In other words, for each noise level D, this figure represents the optimal modulation period T^* that maximizes the SNR against the noise-related time scale $t_m^f(D)$. Perfect matching corresponds to the diagonal and is necessarily satisfied at $A=0$. However, at larger values of A, the curves are situated above the diagonal, confirming that the optimal periods are larger than $t_m^f(D)$, and furthermore that this difference increases with the modulation amplitudes.

To check whether this amplitude-dependent effect is related to the membrane potential modulation amplitude, the same quantity, i.e., the optimal modulation period, was also computed when A was adjusted so as to maintain $A' = A\tau/\sqrt{1+(\Omega\tau)^2}$ constant. The results are represented in the middle panel of Fig. 16. For low modulation amplitudes, the SNR displays a hump for T always near $t_m^f(D)$ (indicated by the arrow). However, this peak progressively disappears as the modulation amplitude is increased. Therefore, unlike in the time domain, perfect matching is not achieved when A' is held constant.

B. For fixed T

One of the most widely used criteria to characterize SR has been that the peak of the PSD at the modulation period or an SNR derived from it is maximal at some intermediate noise level. Bulsara *et al.* examined this question in the periodically modulated perfect integrator [12]. However, since this system does not have a subthreshold regime, their results cannot be extended directly to the LIFM. Plesser and Tanaka [10] showed that the SNR of the periodically modulated LIFM is maximal at some intermediate noise intensity. In this section, we evaluate the SNR over a wide range of parameters and compute the optimal noise value that maximizes this quantity with the one that would yield time-scale matching.

Figure 17 and Fig. 18 show the ISI distributions (left column in Fig. 17), the PSDs (right column in Fig. 17), F (left column in Fig. 18), and SNR (right column in Fig. 18) for $A=0$ (first row from top), $A=0.001$, 0.01, and 0.05 (from second to fourth row).

The main influence of noise on the PSD is to increase the base value at large frequencies, since large noise levels lead to shorter mean ISI $\langle t \rangle$ and hence large $1/\langle t \rangle$. Due to this effect, P_M increases monotonously for low modulation amplitudes.

The graph of D versus P_M does not display any resonance (see $A=0.05$ in the lower panel of Fig. 19). This phenomenon is also apparent in the upper panels of the right column of Fig. 17. At larger modulation amplitudes, the situation is different. The size of the peak at the modulation frequency grows at low noise levels, goes through a maximal value, and then decays. The lowest panel in the right column of Fig. 17 shows how the shape of the PSD changes in this process. When the corresponding profile of P_M is plotted against noise intensity (lower panel of Fig. 19), it appears that in fact the optimal noise level that maximizes P_M is considerably smaller than the one leading to time-scale matching (indicated by the arrow). Thus, this resonance phenomenon that occurs at intermediate subthreshold modulation and low noise levels cannot be attributed to the matching between the time scales of the noise-induced firing and the modulation period in the same way as resonances in the time domain could be.

The influence of noise on the SNR differs from that on P_M. Indeed, at low modulation amplitudes, the SNR exhibits a distinct hump, whereas P_M was monotonously increasing.

The right column of Fig. 18 represents $t_m^f(D)/T$ versus the corresponding value of the SNR. Perfect time-scale matching occurs when the SNR has a maximum at $T = t_m^f(D)$. Panels (b) and (d) of Fig. 18 show that, at low modulation amplitudes, the mode of the SNR is close to one. As the modulation amplitude is increased, this local maximum of the SNR disappears [Figs. 18(f), 18(h)]. However, in these regimes, the SNR exhibits another maximum at larger

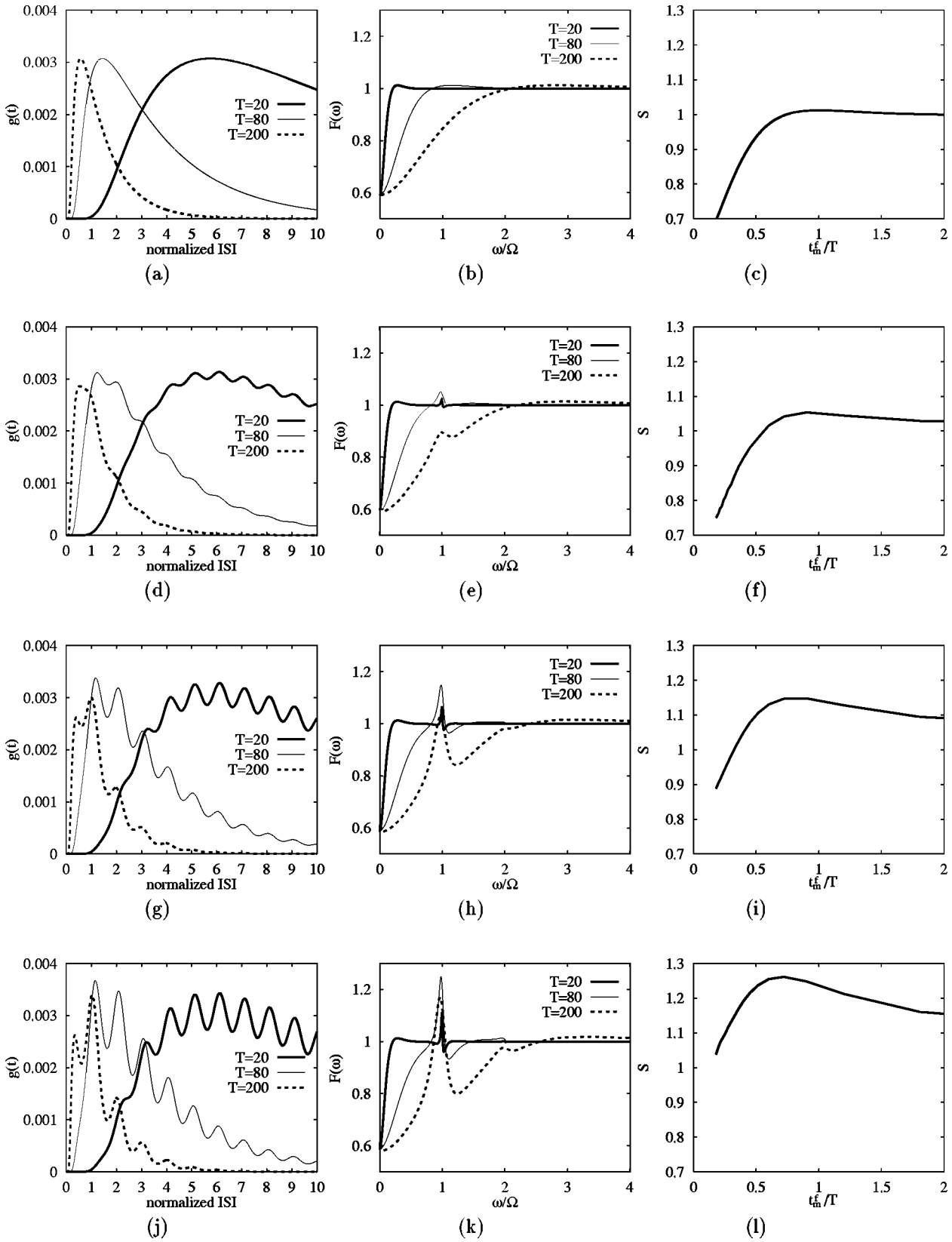

FIG. 15. Left column: abscissa is the ISI normalized by T (dimensionless), and ordinate is the ISI distribution $g(t)$ in kilohertz. Middle column: abscissa is angular frequency ω normalized by modulation angular frequency Ω of the stimulation (dimensionless), and ordinate is $F(\omega)$ (dimensionless). Right column: abscissa is $t_m^f = 2\pi/\omega_m^f$ normalized by the modulation period T (dimensionless), and ordinate is the SNR $S(\omega)$ (dimensionless) for fixed $D = 0.6$ mV while varying T. ω_m^f is the mode of the PSD (or equivalently F) without modulation. Modulation amplitude is $A = 0$ V/s (first row from top), $A = 0.01$ V/s (second row), $A = 0.03$ V/s (third row), and $A = 0.05$ V/s (fourth row). Parameters: $S_0 = 20$ mV, $V_0 = 0$ mV, $D = 0.6$ (mV)^2, $\mu = 0.1$ V/s, $\tau = 1/0.006$ ms.

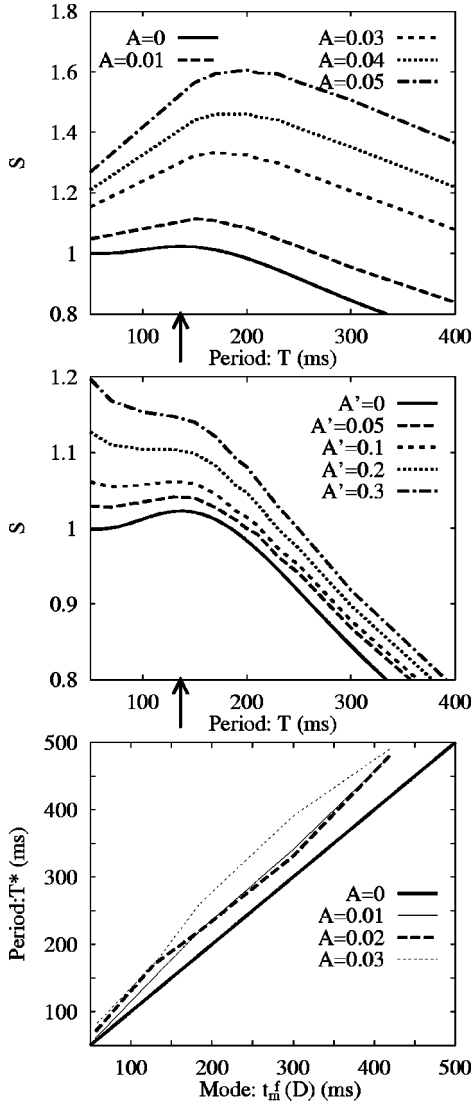

FIG. 16. The two upper panels: the SNR for fixed $D=0.3$ $(\mathrm{mV})^2$. Abscissae are modulation period T in milliseconds. Ordinates are SNR S (dimensionless). Every graph in the upper panel is depicted for fixed A, but in middle panel, $A'=A\tau/\sqrt{1+(\Omega\tau)^2}$ is fixed instead of A. The arrow on the abscissa of both panels points to $t_m^f=136.5$ ms. Lower panel: time-scale matching for endogenous periodic signal in frequency domain. Abscissa is $t_m^f(D)=2\pi/\omega_m(D)$ in milliseconds. $\omega_m(D)$ is the value which gives the maximum of the PSD as a function of ω for fixed D. Ordinate is the optimal modulation period T^* in milliseconds. It gives the maximum of the SNR as a function of T (or ω) for fixed D. Parameters: $\mu=0.1$ V/s, $\tau=1/0.006$ ms, $S_0=20$ mV, $V_0=0$ mV.

$t_m^f(D)$, that is, at lower noise intensity. This second hump cannot be attributed to time-scale matching as it occurs for small noise levels.

The two upper panels of Fig. 19 show the difference in the shape of the SNR at low and large (but still subthreshold) modulation amplitudes. In both panels, the arrow indicates the noise level such that $t_m^f(D)=T$. For A small, the SNR has a hump for some D near the arrow. Still, the SNR at lower noise levels can be larger than this local maximum. Another hump appears at a lower noise level. The optimal value of D that leads to this maximal value varies little with A, however, the peak value itself increases with A.

VI. DISCUSSION

We considered the response of the LIFM to subthreshold periodic stimulation in the presence of additive noise. We used both time domain and frequency domain criteria for the evaluation of the response. Most of these criteria go through a maximum when either noise amplitude or modulation period are varied, thus displaying a ''resonancelike'' hump shaped curve. We examined whether these maxima occurred when some characteristic time scale of noise-induced firing matched the modulation period.

In the time domain, as in [9], we used the mode of the ISI distribution in the absence of the modulation as the relevant time scale for the noise-induced firing. In the frequency domain, we used the mode of the PSD.

These choices revealed time-scale matching for low modulation amplitudes, in both time and frequency domains, when the period T was the tuning parameter. Furthermore, they showed that taking into account the period-dependent changes in the membrane potential oscillation amplitudes increased the range of input amplitudes for which time-scale matching was associated with the optimal response of the LIFM.

When the noise D was the tuning parameter, time-scale matching held only approximately. In the time domain, it improved when the stimulation amplitude was increased, while in the frequency domain, the response of the system was more complex. Indeed, for low modulation amplitudes, the SNR was maximal for an optimal noise level close to the one leading to time-scale matching. However, as the signal amplitude was increased, this maximum disappeared. For these ranges of modulation amplitudes, the SNR presented a maximum at a significantly lower noise intensity. In other words, there are two types of noise-enhanced response in the frequency domain: one for low modulation amplitudes at noise levels close to time-scale matching, and the other for intermediate modulation amplitudes, at low noise intensities. Our numerical investigations (not shown) indicate that the hump discovered by Plesser and Tanaka [10] belongs to the latter class.

When the matching with the mode was far from perfect, or deteriorated through the change of a parameter, such as the modulation amplitude, we examined whether other noise-related time scales, such as the mean ISI in the time domain, did not provide better matching. However, in all cases, these yielded less satisfactory results than the modes (not shown). Therefore, at this point, it is not possible to pin down a simple explanation in terms of time-scale matching for noise-enhanced signal transmission when the modes did not match, even approximately, the modulation period. These need to be investigated on their own, and are probably dependent on the interplay between the time scales and amplitude-dependent factors.

Our study revealed significant differences that appear when considering the response of the system in time and frequency domains. The optimal modulation periods or noise intensities that maximize the response of the system in time and frequency domain are different. This stems from the fact

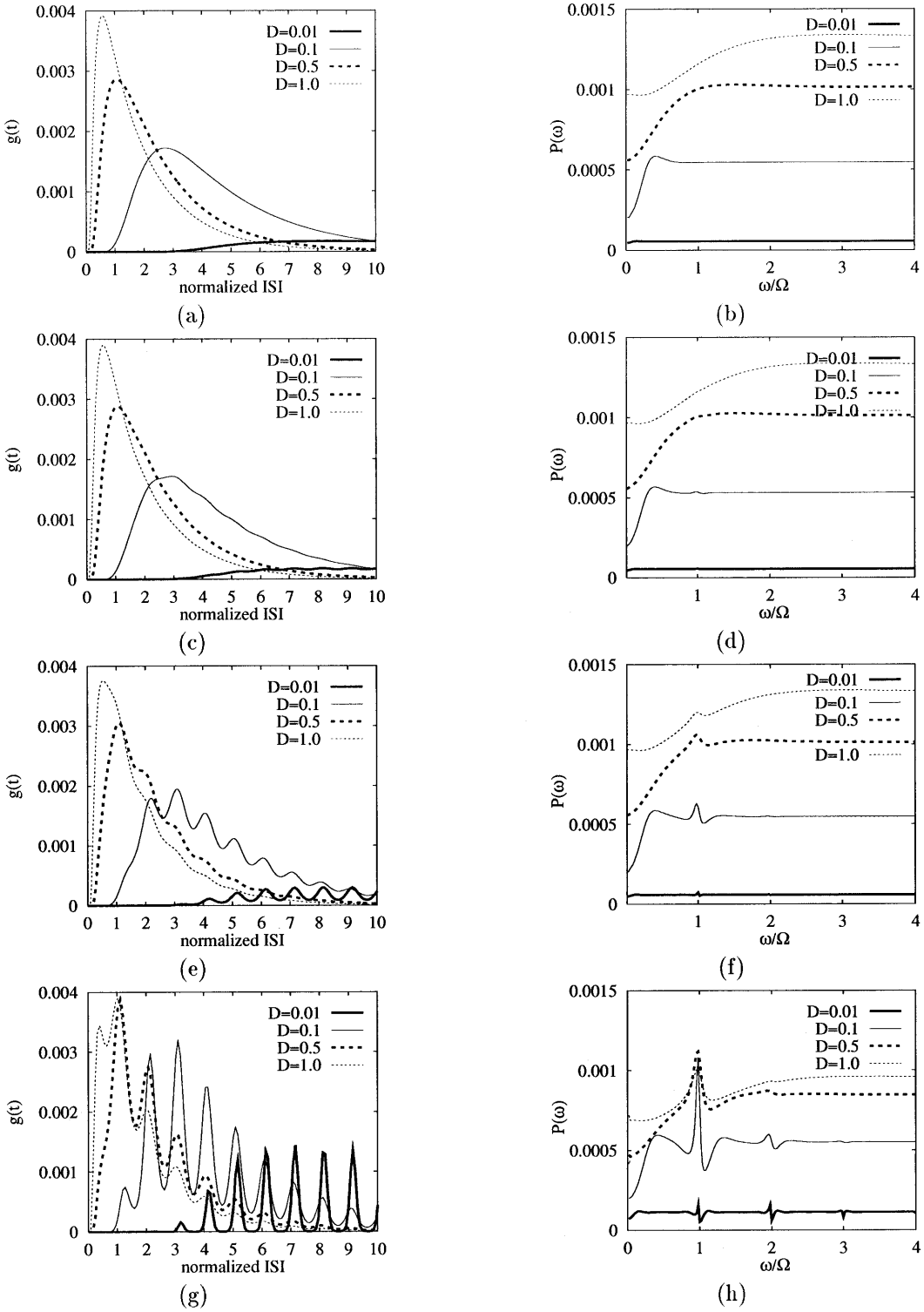

FIG. 17. ISI distribution (left column) and corresponding PSD (right column) for four different noise levels D for four modulation amplitudes $A=0$ V/s (first row from top), $A=0.001$ V/s (second row), $A=0.01$ V/s (third row), and $A=0.05$ V/s. Abscissae of left column: ISI normalized by T (dimensionless); ordinate of left column: the ISI PDF $g(t)$ in kilohertz. Abscissae of right column: angular frequency ω normalized by stimulation angular frequency Ω (dimensionless); ordinate of right column: the PSD $P(\omega)$ in kilohertz. Parameters: $S_0=20$ mV, $V_0=0$ mV, $\mu=0.1$ V/s, $\tau=1/0.006$ ms, $T=2\pi/0.05$ ms.

that the criteria used to assess the regularity of the system's response in time and frequency domains are sensitive to different aspects of the spike train. Nevertheless, all criteria show that tuning the modulation period or the noise intensity can improve the response to weak stimuli. The differences between time domain and frequency domain criteria grow with the modulation amplitude.

Furthermore, we introduced a method in order to compute the ISI distribution when the phase of the input is not reset at each discharge. The comparison between this case and the

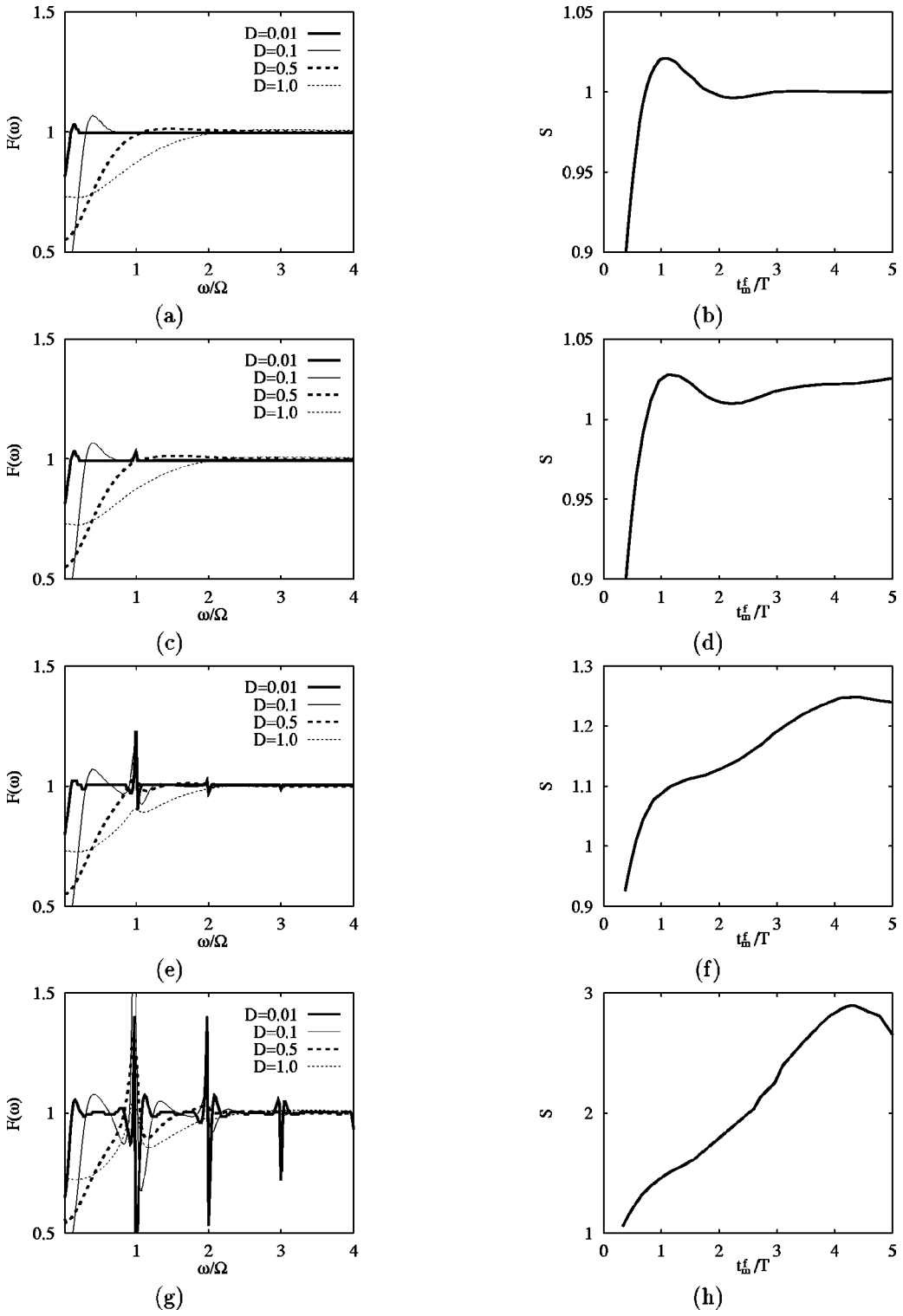

FIG. 18. Left column: the function $F(\omega)$ for four different noise levels D for four modulation amplitudes $A=0$ V/s (first row from top), $A=0.001$ V/s (second row), $A=0.01$ V/s (third row) and $A=0.05$ V/s. Abscissae: angular frequency ω normalized by stimulation angular frequency Ω (dimensionless); ordinates: $F(\omega)$ (dimensionless). Right column: SNR for fixed $T=2\pi/0.05$ ms while varying D against $t_m^f(D)/T$ with $t_m^f=2\pi/\omega_m^f$ where ω_m^f is the mode of the PSD (or equivalently F) without modulation. Abscissa: t_m^f normalized by the modulation period T (dimensionless); ordinate: the SNR $S(\omega)$ (dimensionless). The parameters are the same as in Fig. 17.

endogenous situation revealed that the latter could be used as a satisfactory approximation of the former for the evaluation of time-scale matching, as long as the input amplitude is weak. This is in agreement with [9]. The advantage of this approximation is its numerical and analytical tractability. The computation of the cycle histogram confirms the validity of the approximation for weak modulation and low noise levels where it displays a sharp peak. When the modulation

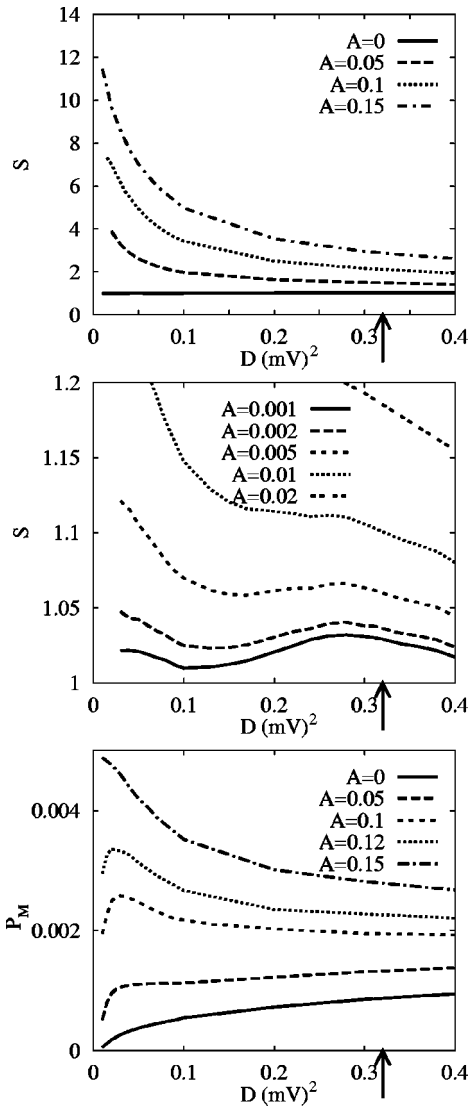

FIG. 19. Two upper panels: abscissa: noise intensity D in millivolts; ordinate: the SNR S (dimensionless). The ordinate of the middle panel is the magnification of that of the upper panel. Arrows on both abscissae point to $D=0.32$ (mV)^2 such that the mode of the PSD equals T. Lower panel: abscissa: noise intensity D in (millivolts)^2; ordinate: the maximum value P_M, in kilohertz, of the PSD near Ω. All figures are the case for fixed $T=2\pi/0.05$. Parameters: $S_0=20$ mV, $V_0=0$ mV, $\mu=0.1$ V/s, $\tau=1/0.006$ ms, $T=2\pi/0.05$ ms.

period is slow compared to the membrane charge-discharge time, the peak is situated close to $\pi/2$, suggesting that the choice of this phase as the resetting phase gives satisfactory results. Numerical investigations confirm this point.

VII. CONCLUSION

Experimental investigations have shown that noise of appropriate amplitude can improve signal transmission and processing in sensory neurons. Some of these have reported SR-like phenomena, that is, when noise helps the detection of weak signals. On the one hand, these studies show that quantities such as the value of the interspike interval distribution, the signal-to-noise ratio, the input-output correlation, transinformation, or coherence are maximized at some intermediate noise level. Theoretical investigations using neuron models, on the other hand, have helped in clarifying the conditions under which such phenomena occur, as well as the mechanisms underlying them. One issue of particular interest has been whether the same putative mechanism that leads to SR in weakly periodically modulated bistable systems, namely, matching between the time scales of the noise-induced hopping and the modulation period, is also responsible for noise-enhanced signal transmission in sensory neurons. Following [9,10], this work investigated this question in the case of the LIFM. Our analysis suggests that time-scale matching occurs when at low modulation amplitudes the modulation period is tuned to maximize the system's response. It also holds, approximately, when the noise amplitude is tuned. Our investigations also showed that time-scale matching is not the only process responsible for noise-induced response improvement, as for intermediate modulation amplitudes, the SNR is maximal at noise intensities much lower than the ones leading to time-scale matching.

ACKNOWLEDGMENTS

The authors would like to thank Dr. A. Bulsara and Dr. S. Lowen for helpful discussions.

APPENDIX: COMMENTS FOR NUMERICAL CALCULATION

In order to numerically evaluate the integrals in the algorithm to calculate the t_{FP} PDF [15], we used time steps smaller than both τ and $T/50$. Furthermore, for large D, the time step was smaller than $t_m/10$ where t_m was the mode of the t_{FP} PDF. In order to set the time step appropriately while changing T or D, we calculated first the t_{FP} PDF for the minimum T or maximum D and checked whether controls computed with smaller steps yielded similar results. Then this value was used throughout the computation for all values of T and D.

To examine time-scale matching for the endogenous periodic signal, calculations of the t_{FP} PDF were stopped at the modulation period. However, to compute either the ISI distribution for exogenous periodic signals or the PSD of the spike train and the corresponding SNR for endogenous periodic signals, calculations of the t_{FP} PDF were stopped when the area below the curve of g, that is, $\int_0^t g(t)dt$, became larger than 0.9999. We estimated this area using the trapezoidal method.

In the computation of the PSD, we calculated the Fourier transform of the t_{FP} PDF using the fast Fourier transform algorithm.

[1] J. P. Segundo *et al.*, in *Origins: Brain and Self Organization*, edited by K. Pribram (Lawrence Erlbaum Associates Publisher, Hillsdale, NJ, 1994).
[2] J. E. Levin and J. P. Miller, Nature (London) **380**, 165 (1996); J. J. Collins, C. C. Chow, and T. T. Imhoff, *ibid.* **376**, 236 (1995); J. J. Collins *et al.*, J. Neurophysiol. **76**, 642 (1996); J. J. Collins *et al.*, Phys. Rev. E **52**, R3321 (1995); J. J. Collins *et al.*, *ibid.* **54**, 5575 (1996); D. R. Chialvo, A. Longtin, and J. Müller-Gerking, *ibid.* **55**, 1798 (1997); J. Murakami, T. Shimozawa, and Y. Baba, IEICE Technical Report No. MBE96-28, 1996 (in Japanese).
[3] J. K. Douglass *et al.*, Nature (London) **365**, 337 (1993).
[4] D. R. Chialvo and A. V. Apkarian, J. Stat. Phys. **70**, 375 (1993); A. Longtin, *ibid.* **70**, 309 (1993); A. Longtin, A. R. Bulsara, and F. Moss, Phys. Rev. Lett. **67**, 656 (1991); X. Pei, K. Bachman, and F. Moss, Phys. Lett. A **206**, 61 (1995); A. Longtin *et al.*, Biol. Cybern. **70**, 569 (1994).
[5] A. R. Bulsara and L. Gammaitoni, Phys. Today **49** (3), 39 (1996); F. Moss, D. Pierson, and D. O'Gorman, Int. J. Bifurcation Chaos Appl. Sci. Eng. **4**, 1383 (1994).
[6] L. Gammaitoni *et al.*, Rev. Mod. Phys. **70**, 223 (1998).
[7] L. Gammaitoni, F. Marchesoni, and S. Santucci, Phys. Rev. Lett. **74**, 1052 (1995); M. H. Choi, R. F. Fox, and P. Jung, Phys. Rev. E **57**, 6335 (1998).
[8] K. Wiesenfeld *et al.*, Phys. Rev. Lett. **72**, 2125 (1994).
[9] A. R. Bulsara *et al.*, Phys. Rev. E **53**, 3958 (1996).
[10] H. E. Plesser and S. Tanaka, Phys. Lett. A **225**, 228 (1997).
[11] P. Lánský, Phys. Rev. E **55**, 2040 (1997).
[12] A. R. Bulsara, S. Lowen, and C. Rees, Phys. Rev. E **49**, 4989 (1994).
[13] J. P. Keener, F. C. Hoppensteadt, and J. Rinzel, SIAM (Soc. Ind. Appl. Math.) J. Appl. Math. **41**, 503 (1981).
[14] L. M. Ricciardi, *Diffusion Processes and Related Topics in Biology*, Lecture Notes in Biomathematics Vol. 14 (Springer-Verlag, Berlin, 1977); S. Sato and L. M. Ricciardi, in *Lectures in Applied Mathematics and Informatics*, edited by L. M. Ricciardi (Manchester University Press, New York, 1990).
[15] V. Giorno *et al.*, Adv. Appl. Probab. **21**, 20 (1989).
[16] S. Sato, J. Appl. Probab. **14**, 850 (1977).
[17] T. Tateno *et al.*, J. Stat. Phys. **78**, 917 (1995); S. Doi, J. Inoue, and S. Kumagai, *ibid.* **90**, 1107 (1998); T. Tateno, *ibid.* **92**, 675 (1998).
[18] T. Shimokawa *et al.*, IEICE Technical Report No. MBE97-14, 1997 (in Japanese).
[19] A. Lasota and M. C. Mackey, *Chaos, Fractals and Noise—Stochastic Aspects of Dynamics* (Springer-Verlag, New York, 1994).